nature
cell biology

elipsa is an early determinant of ciliogenesis that links the IFT particle to membrane-associated small GTPase Rab8

Yoshihiro Omori[1], Chengtian Zhao[1], Arunesh Saras[1], Saikat Mukhopadhyay[2], Woong Kim[2], Takahisa Furukawa[4], Piali Sengupta[2], Alexey Veraksa[3], Jarema Malicki[1,5]

The formation and function of cilia involves the movement of intraflagellar transport (IFT) particles underneath the ciliary membrane, along axonemal microtubules[1,2]. Although this process has been studied extensively, its molecular basis remains incompletely understood. For example, it is unknown how the IFT particle interacts with transmembrane proteins. To study the IFT particle further, we examined *elipsa*, a locus characterized by mutations that cause particularly early ciliogenesis defects in zebrafish. We show here that *elipsa* encodes a coiled-coil polypeptide that localizes to cilia. Elipsa protein binds to Ift20, a component of IFT particles, and Elipsa homologue in *Caenorhabditis elegans,* DYF-11, translocates in sensory cilia, similarly to the IFT particle. This indicates that Elipsa is an IFT particle polypeptide. In the context of zebrafish embryogenesis, Elipsa interacts genetically with Rabaptin5, a well-studied regulator of endocytosis, which in turn interacts with Rab8, a small GTPase, known to localize to cilia. We show that Rabaptin5 binds to both Elipsa and Rab8, suggesting that these proteins provide a bridging mechanism between the IFT particle and protein complexes that assemble at the ciliary membrane.

Cilia are specialized organelles on the cell surface that generate fluid flow and sense environmental changes. Sensory cilia contain molecules involved in signal detection and transduction, such as Rhodopsin, olfactory receptors, Smoothened, TRP channels or the PDGF receptor[3,4]. These transmembrane proteins are produced in the endoplasmic reticulum and transported via cytoplasmic vesicles to the base of the cilium. In the cilium itself, membrane proteins are thought to be translocated in association with IFT particles[2], which consist of at least 15 proteins that are assembled in two complexes named A and B. In many species, mutations that eliminate IFT components cause loss of cilia[5]. IFT particles are observed by electron microscopy as electron-dense

structures tightly sandwiched between axonemal microtubules and the cell membrane. The speed of their movement along ciliary microtubules can be determined using video recordings[1,6]. Although IFT-particle motility is driven by microtubule-dependent motors, the IFT particle itself is thought to drive the movement of other proteins, including those deposited in the ciliary membrane. The six-pass transmembrane proteins that form the TRPV channel, for example, translocate in cilia with the speed characteristic of the IFT particle, and their distribution is defective in *IFT* mutants[7]. Here we show that Elipsa is a component of the IFT particle that has not been identified in previous studies. Elipsa binds directly to the Ift20 polypeptide and also interacts genetically with Rabaptin5. Elipsa binds to Rabaptin5, which, in turn, binds to Rab8, a membrane-associated small GTPase, thus potentially providing a bridging mechanism between IFT transport and membrane-associated protein complexes.

We showed previously that in zebrafish *IFT* mutants, cilia were initially present at approximately 30 h postfertilization (hpf), but failed to be maintained[5]. *elipsa* larvae exhibit abnormalities characteristic of mutants with defective cilia[8,9], such as curly body axis, and kidney cysts (Fig. 1a, b and data not shown), but display an even earlier defect in ciliogenesis (Fig. 1c'–g'). To determine the molecular nature of *elipsa*, we showed that it maps to the linkage group 9 between the markers z8363 and z10789. A large group of cilia-related genes were identified based on genome comparisons of ciliated and non-ciliated organisms[10]. We noticed that a gene from this group maps to the *elipsa* genomic region. Sequencing of the open reading-frame from *elipsa* mutants revealed defects, including a single amino acid substitution in the *eli*[m649] allele and a premature stop codon in *eli*[tp49d] (Fig. 1h, k). The substitution in *eli*[m649] affects an amino (N)-terminal isoleucine conserved in a broad range of species, including human and *C. elegans* (Supplementary Information, Fig. S1a–c), whereas the premature stop codon in *eli*[tp49d] causes truncation of approximately two-thirds of the Elipsa protein. The injection
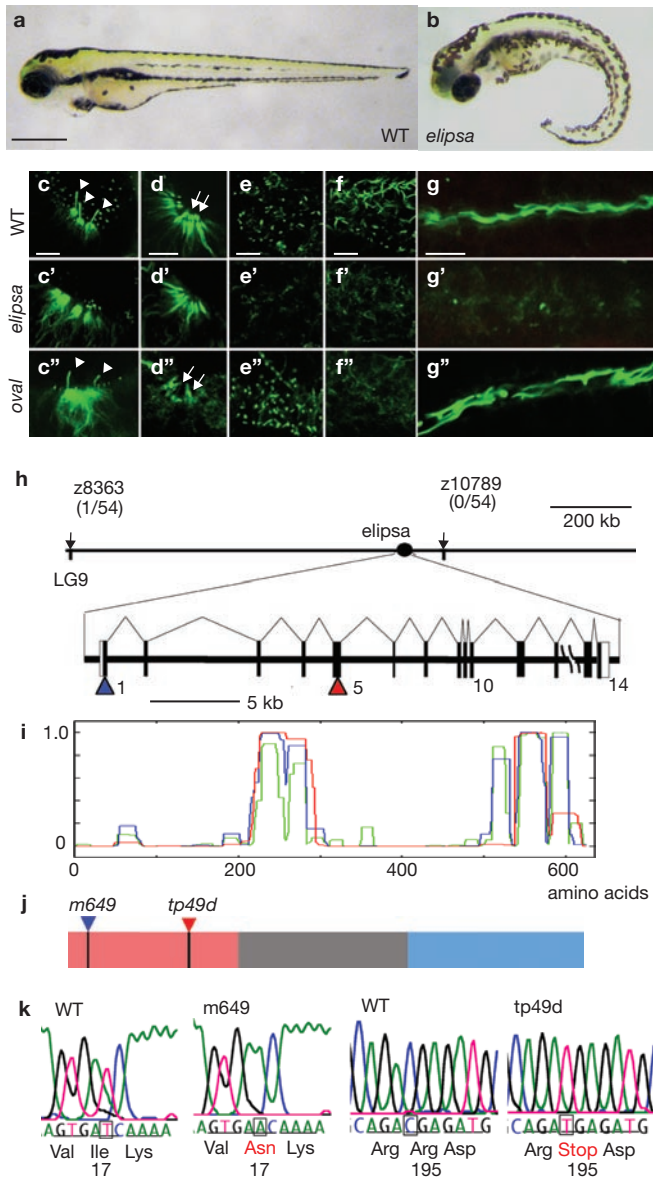
Figure 1 The *elipsa* phenotype and gene structure. (**a**, **b**) Wild-type (WT, **a**) and *elipsa* mutant (**b**) zebrafish larvae at 3 dpf. Anterior is left, dorsal is up. (**c**–**g′′**) Staining of cilia with anti-acetylated α-tubulin antibodies in the otic vesicle (**c**–**c′′**), olfactory placode (**d**–**d′′**), the apical surface of the retinal neuroepithelium (**e**–**e′′**, tangential optical sections), the spinal canal (**f**–**f′′**) and the pronephric duct (**g**–**g′′**). Staining of WT (30 hpf), *elipsa* (30 hpf) and *oval* (40 hpf) mutant animals. (**h**) Genetic map of the *elipsa* locus and the exon/intron structure of the *elipsa* transcript. (**i**) The distribution of coiled-coil regions in the Elipsa polypeptide as determined by COILS software, version 2.1. (**j**) The defect in the *tp49d* mutant allele introduced a premature termination codon, whereas the *m649* mutation produced a substitution of a highly conserved Ile (Supplementary Information, Fig. S1). Conserved regions are coloured as in Supplementary Information, Fig. S1c. (**k**) Sequencing trace data for the two *elipsa* mutant alleles. Scale bars are 500 μm (**a**) and 10 μm (**c**–**g**).

of anti-*elipsa*-ATG morpholino antisense oligonucleotides (MOs) into wild-type embryos produced the *elipsa* defect, whereas the injection of *elipsa* mRNA into *elipsa* homozygous mutant embryos restored the wild-type phenotype (see Supplementary Information, Tables S1, S2, Fig. S2 for details). Taken together, these results provide conclusive evidence that we have identified the molecular nature of the *elipsa* gene.

The *elipsa* gene (genbank: EU117166) encodes a polypeptide of 629 amino acids and is well conserved in genomes of diverse phyla (Supplementary Information, Fig. S1). Its sequence lacks obvious motifs, except for two predicted coiled-coil regions found roughly between amino acids 200–300 and 500–600 (Fig. 1i). The N- and carboxy (C)-termini are better conserved than the middle portion of the protein. The N-terminal region of approximately 130 amino acids and the C-terminal region of approximately 110 amino acids are approximately 80% identical to the human sequence (colour-coded in Fig. 1j; Supplementary Information, Fig. S1c). Consistent with its mutant phenotype, the *elipsa* transcript was particularly enriched in ciliated tissues, including olfactory pits, lateral line organs and pronephric ducts (data not shown). The Elipsa–GFP fusion protein suppressed the body curvature and kidney phenotypes of *elipsa* mutant animals (Supplementary Information, Table S2), and localized to basal bodies in several tissues, including the retina, the otic vesicle and the olfactory epithelium (Fig. 2a–c). Although more difficult to detect, it was also present in the axoneme of otic and nasal cilia (Fig. 2d–g). This localization is consistent with a role of *elipsa* in ciliogenesis.

To identify potential binding partners of Elipsa, we performed a yeast two-hybrid screen with the full-length Elipsa, as well as with its C-terminal fragment of 300 amino acids as baits. The screening of 2×10^6 and 0.5×10^6 transformants with the first and second baits, respectively, identified four independent clones of *ift20* and two independent clones of *rabaptin5*. Ift20 is a component of the IFT particle, whereas Rabaptin5 is a coiled-coil protein that functions as an effector of small Rab-family GTPases and enhances endocytic vesicle fusion[11,12]. Deletion analysis indicated that an evolutionarily conserved C-terminal coiled-coil region of approximately 90 amino acids in the Elipsa polypeptide (Supplementary Information, Fig. S1) was sufficient to mediate its interaction with Ift20 (Fig. 3a, b). A strong interaction of Elipsa with Ift20 was also detectable on Coomassie-stained gels (data not shown) and on western blots following pulldown assays of MBP–Ift20 with GST–Elipsa (Fig. 3e). These experiments provide compelling evidence that Elipsa binds to Ift20.

To confirm yeast two-hybrid and *in vitro* binding data and to isolate additional Elipsa-binding partners, we performed tandem affinity purification (TAP) using Elipsa as bait. This approach has been applied previously in several model systems, including *Drosophila melanogaster* and *C. elegans*, but to our knowledge has not been used in zebrafish. To perform TAP, we tagged Elipsa with green fluorescent protein (GFP) at the N-terminus and with a TAP-tag at the C-terminus (Fig. 3c). A GFP polypeptide fused to a TAP-tag was used as a negative control. mRNAs encoding these fusion proteins were generated *in vitro* and injected into zebrafish embryos. At 30 hpf, embryos were collected to prepare extracts for TAP. The resulting purification products were separated on a polyacrylamide gel (Fig. 3d) and analysed using mass spectrometry. This procedure identified six IFT-particle-associated proteins as Elipsa-interacting partners: Ift20, Ift57, Qilin, Ift80, Ift81 and Ift172 (Fig. 3d; Supplementary Information, Table S3). These results confirm our yeast two-hybrid data and indicate that Elipsa interacts with complex B of the IFT particle.

To test whether the localization of the Elipsa polypeptide depends on IFT-particle components, we analysed its distribution in *oval/ift88* mutants and in *ift20* morphants. Ift20–GFP fusion protein localized to the basal body region (Fig. 3f, g) and a knockdown of *ift20* gene function caused curling of the body axis (Supplementary Information,
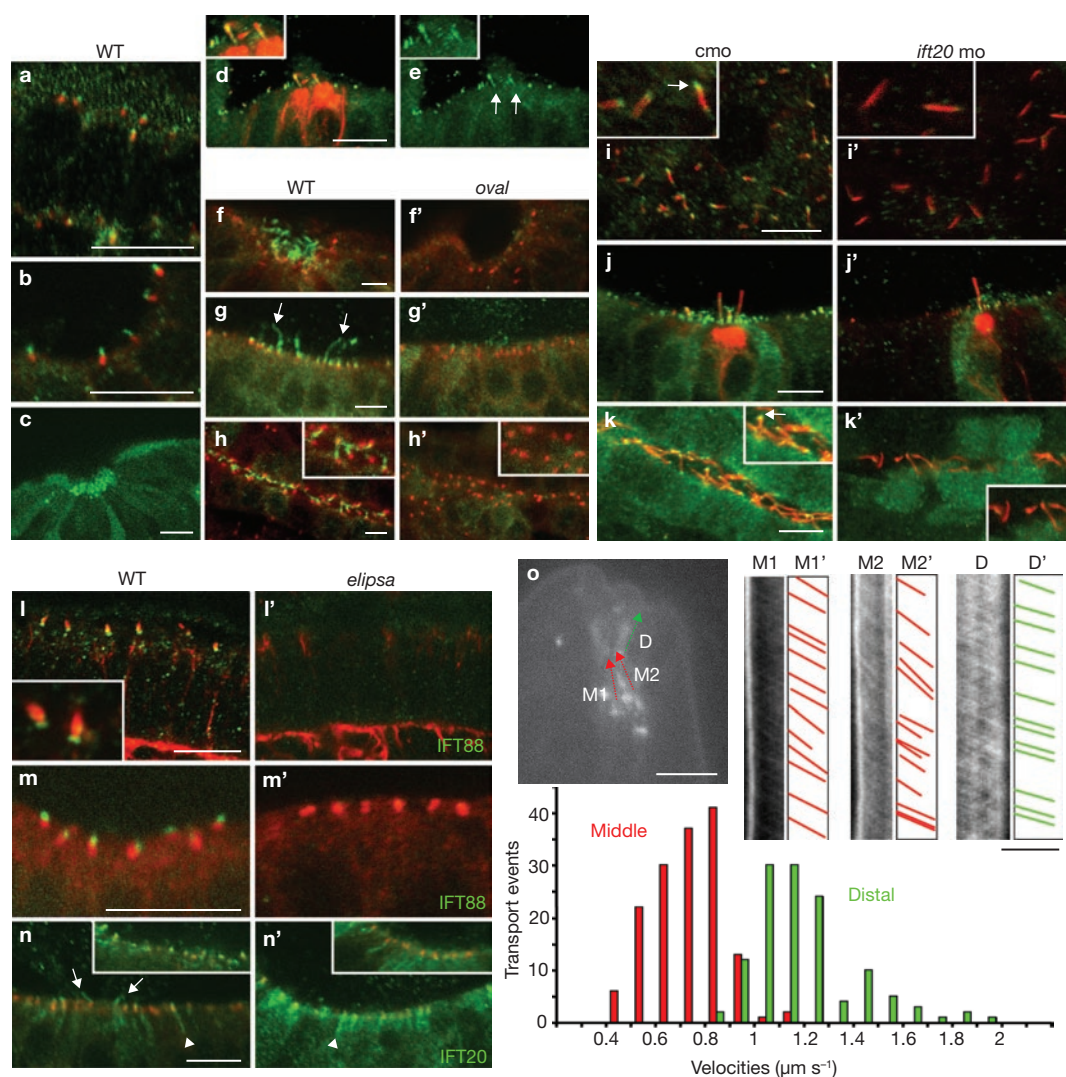
Figure 2 Localization of Elipsa and IFT proteins. (**a–k′**) Embryos expressing Elipsa–GFP fusion protein stained with anti-GFP antibody (green). Shown are photoreceptor connecting cilia at 60 hpf (**a**), the otic vesicle cilia (**b**) and olfactory pit cilia (**c**) at 48 hpf. (**d**, **e**) Elipsa–GFP was enriched in hair-cell kinocilia (arrows in **e**, magnified in the inset) at 60 hpf. (**f–h′**) Staining of the olfactory pit (**f**, **f′**), the otic vesicle epithelium (**g**, **g′**) and the pronephric duct (**h**, **h′**) in the WT (left panels) and *oval* (right panels) embryos. Arrows in (**g**) indicate Elipsa–GFP expression in cilia. (**i–k′**) Apical surface staining in the retinal neuroepithelium (**i**, **i′**, tangential optical sections), the otic vesicle epithelium (**j**, **j′**) and the pronephric duct (**k**, **k′**) in control (left panels) and *ift20* (right panels) morphants. Arrows in **i** and **k** insets indicate Elipsa localization at the base of cilia. (**l–n′**) Staining of the photoreceptor cell layer (**l**, **l′**), and the otic vesicle epithelium (**m–n′**), in WT (left panels) and *elipsa* (right panels) embryos, with anti-Oval/Ift88 (**l–m′**) or anti-GFP (**n**, **n′**)

antibodies. Embryos in **n**, **n′** expressed Ift20–GFP fusion protein, detected in cilia (arrows) as well as in more basal regions of the cell (arrowheads). Insets show another example of this staining pattern. Embryos in (**a–n**) were counterstained in red with antibodies to γ-tubulin (**a**, **b**, **f–h′**, **m–n′**) or acetylated α-tubulin (remaining panels). Scale bars are 10 μm. (**o**) Anterograde transport of GFP-tagged C02H7.1 in the cilia of *C. elegans* sensory neurons. Shown are a still image (upper left; scale bar is 5 μm) and kymographs (upper right; horizontal scale bar is 5 μm; vertical is 5 s) from a representative movie of C02H7.1 transport. Histograms of C02H7.1–GFP velocities are shown at the bottom. Kymographs were generated along lines indicated with arrows in the middle (M1, M2, red) and distal (D, green) segments and used to calculate velocities. The average velocities were 0.73 ± 0.14 μm sec⁻¹ in middle segments (152 particles per 5 cilia examined), and 1.20 ± 0.21 μm sec⁻¹ in the distal segment (124 particles per 5 cilia examined).

Fig. S3b) with loss of cilia that somewhat preceded that seen in *oval/ift88* animals (Supplementary Information, Fig. S3e′–g′). We found that Elipsa no longer localized to basal bodies in the *oval* mutant (Fig. 2f′–h′, green signal) or in *ift20* morphant animals (Fig. 2i′–k′, green signal). Conversely, the localization of both Oval/Ift88 and Ift20 required Elipsa (Fig. 2l′–n′). Thus Elipsa and IFT-particle components are reciprocally dependent on each other for their proper intracellular localization, further supporting the notion that Elipsa is closely associated with the IFT particle.

A hallmark of IFT-complex components is their ability to translocate along the ciliary shaft. To investigate whether Elipsa translocates in a manner similar to that of IFT particles, we performed studies in *C. elegans*, a well-established system for studies of IFT-particle motility[6]. The genomic location of *C02H7.1* (the *C. elegans* homologue of *elipsa*) corresponds closely to the genetic map position of the previously identified *dyf-11* (dye-filling defective) locus[13]. *dyf-11* mutants were isolated on the basis of their inability to fill a subset of sensory neurons with lipophilic dye, a trait characteristic of ciliary
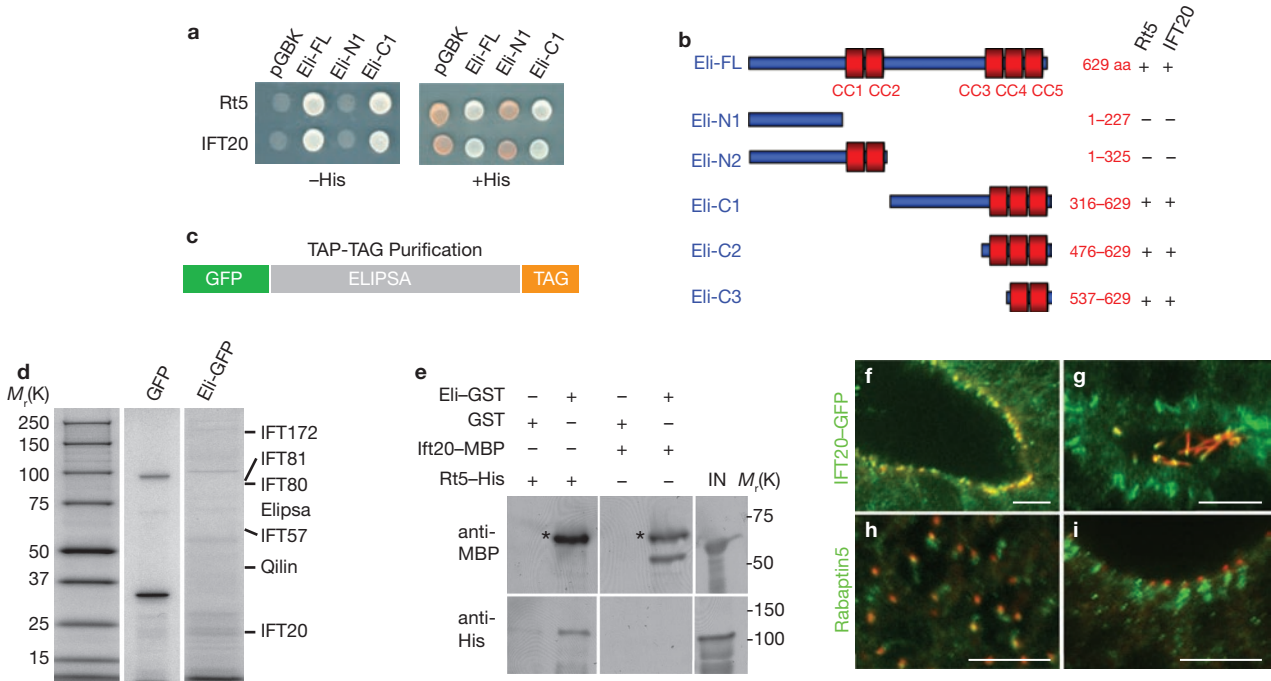
439

Figure 3 Elipsa binding partners. (**a**) Yeast two-hybrid tests for binding interactions of Elipsa with Ift20 and Rabaptin5 (Rt5). Three Elipsa constructs were used in these studies: full-length Elipsa (Eli-FL), Elipsa N-terminal region (Eli-N1) and Elipsa C-terminus (Eli-C1). Only the full-length protein or its C-terminus interacted with Ift20 and Rabaptin5 (His, histidine; pGBK, empty vector control). (**b**) A summary diagram of Elipsa binding to Ift20 and Rabaptin5. A C-terminal region of approximately 90 amino acids was sufficient to mediate Elipsa binding in yeast two-hybrid tests. Coiled-coil regions are indicated in red. (**c**) A schematic representation of Elipsa fusion polypeptide used in TAP experiments; TAG, tandem affinity purification tag. (**d**) Polyacrylamide gel electrophoresis of TAP products. The left lane shows size standards, the middle lane purification using GFP-tag control construct and the right lane shows purification using GFP–Elipsa-tag construct. Most purification products were not detectable on a Coomassie Blue-stained gel, and were identified by staining the gel in sections and performing mass spectrometry. A faint Ift172 band is visible in the Eli–GFP but not GFP lane. (**e**) Western blot analysis of GST pulldown products detected with anti-MBP or anti-HisTag antibodies, as indicated. The input lanes (IN) contained approximately 5% of the protein used in binding assays shown to the left. The asterisk indicates a non-specific band. (**f**, **g**) Anti-GFP antibody staining of cryosections through the brain ventricle (**f**) and the pronephric duct (**g**) of zebrafish larvae expressing Ift20–GFP fusion polypeptide (green) at 36 hpf. (**h**, **i**) Whole-mount anti-Rabaptin5 antibody staining of the apical surface in the retinal neuroepithelium (**h**, tangential optical section) and the otic vesicle epithelium (**i**, optical cross-section). (**f–i**) Specimens were counterstained with anti-acetylated-α-tubulin (**g**, **i**) or anti-γ-tubulin antibodies (**f**, **h**) in red. Scale bars are 10 μm (**f–i**).

structure mutants[13,14], and were also shown to exhibit sensory defects[13,15]. A GFP-tagged full-length C02H7.1 fusion protein fully rescued the dye-filling defect of *dyf-11*(*mn392*) mutants (Supplementary Information, Fig. S4a). Moreover, the *mn392* allele contains a premature stop codon in the third exon of *C02H7.1*, and is predicted to encode a truncated protein of 139 amino acids (Supplementary Information, Fig. S4b). Consistent with data published recently[16], these results indicate that, as seen in zebrafish, mutations in the *elipsa* homologue in *C. elegans* cause ciliary defects. When expressed in sensory neurons, the C02H7.1–GFP fusion protein localized to cilia (Supplementary Information, Fig. S4c) and translocated in the middle and distal cilia segments at velocities approximating those of IFT particle components[6,17] (Fig. 2o; Supplementary Information, Movie 1). Similarly to IFT-complex B proteins, the speed of Elipsa translocation increased in the middle ciliary segment and was similar to that of the distal segment in *bbs-8* mutants (Supplementary Information, Fig. S4d–f)[15]. Given that IFT-particle components are well conserved, even in phyla evolutionarily distant from each other[2], this result suggests that Elipsa may also undergo IFT in zebrafish cilia. Collectively, these experiments indicate that Elipsa functions as a component of the IFT particle.

Unexpectedly, our yeast two-hybrid screen also showed that Rabaptin5 interacts with Elipsa. Rabaptin5 is a Rab effector that has been extensively studied in the context of endocytosis[12,18,19]; however, there is no evidence to date for its role in ciliogenesis. Similarly to Ift20, Rabaptin5 bound to the C-terminal coiled-coil region of 90 amino acids of the Elipsa polypeptide in a yeast two-hybrid assay (Fig. 3a, b). The C-terminal amino acids 489–862 of Rabaptin were sufficient to mediate this interaction. To confirm this result, we performed a pulldown assay using an Elipsa–GST fusion protein. Consistent with previous data, full-length zebrafish Rabaptin5–HisTag bound to Elipsa–GST but not to GST alone (Fig. 3e) and Rabaptin5–MBP (amino acids 546–862) fusion polypeptide bound to Elipsa–GST but not to GST alone (data not shown). In agreement with the protein–protein interaction data, antibody staining showed that Rabaptin5 localizes to the basal bodies of auditory and retinal cilia (Fig. 3h–i). The staining signal seemed to be specific, as it was markedly reduced in *Rabaptin5* MO-knockdown animals (Supplementary Information, Fig. S3i). In contrast to Elipsa, Rabaptin5 distributes in a more diffuse manner and was localized mainly basal to ciliary basal bodies (Fig. 3h, i). A similar basal distribution pattern was also observed in some cilia for the IFT20–GFP fusion protein (Fig. 2n).
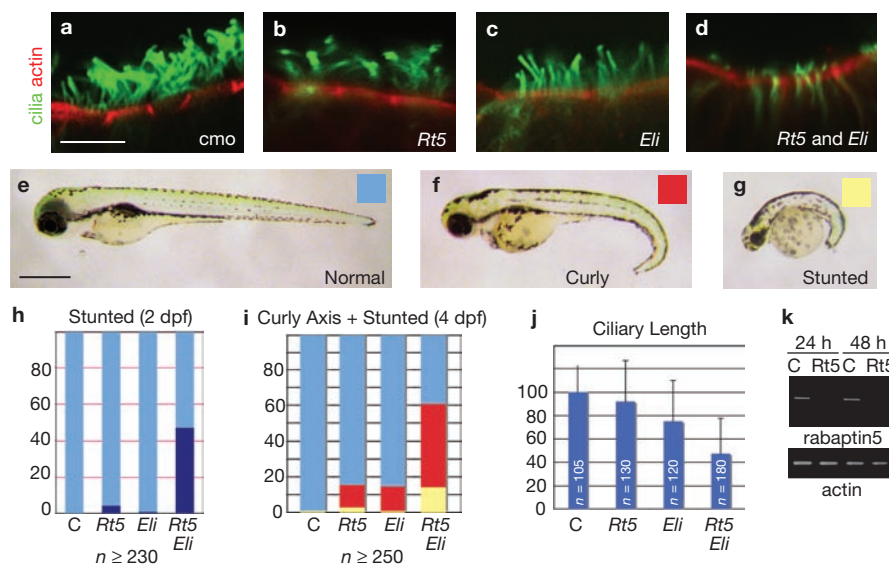
Figure 4 Rabaptin5 interacts genetically with Elipsa and functions in ciliogenesis. (**a**–**d**) Nasal cilia visualized with an anti-acetylated tubulin antibody (green) in embryos treated with the following MOs: cmo, control; *Rt5*, anti-*rabaptin5*; *Eli*, anti-*elipsa*. Embryos were counterstained with phalloidin (red). (**e**–**g**) Phenotype categories of morphant embryos at 4 dpf: normal phenotype (**e**), curly body axis phenotype (**f**) and stunted growth phenotype (**g**). (**h**–**j**) Quantification of phenotypes, as indicated above each graph. The MOs injected are indicated below each graph, abbreviations as above. The bars in **i** are colour-coded as indicated in upper right corners of (**e**–**g**). In **j** the length of olfactory placode cilia was calculated in arbitrary units and expressed as a percentage of the WT value, which was set to 100%. Data are mean ± s. d. (**k**) RT-PCR quantification of anti-*rabaptin5* splice site MO-knockdown efficiency. The WT transcript was not detectable in morphant embryos at 24 and 48 hpf. In (**e**–**g**) anterior is left, dorsal is up. Scale bars are 10 μm (**a**–**d**), and 500 μm (**e**–**g**).

To determine whether Rabaptin5 functions in ciliogenesis, we treated embryos with *rabaptin5* MOs. Knockdown using 1.0 ng nl^{-1} of splice site-targeted MOs caused death of at least 30% of embryos by 24 hpf. The lethality decreased when embryos were treated with 0.2 ng nl^{-1} of oligonucleotides. Surviving embryos usually displayed stunted growth and increased cell death in many tissues. At later stages, we observed a curly-tail phenotype of variable severity, as well as a decrease in the length of olfactory cilia (Fig. 4). The latter two phenotypes resemble defects seen in *IFT* mutant or morphant animals[5] (Fig. 1b; Supplementary Information, Fig. S2b). RT-PCR amplification of the *rabaptin5* transcript from morphant animals did not produce a detectable signal, indicating that the knockdown was efficient (Fig. 4k), whereas the injection of *rabaptin5* mRNA along with an *rabaptin5* MO partially restored wild-type phenotypes, indicating specificity (Supplementary Information, Fig. S3k). To test whether *rabaptin5* and *elipsa* interact genetically, we generated double-morphant animals using a low concentration of both *rabaptin5* (0.2 mg ml^{-1}) and *elipsa* (0.8 mg ml^{-1}) MOs. The overall appearance of the entire embryo and cilia formation were scored. Simultaneous silencing of both genes caused a synergistically more severe phenotype, compared with single-knockdown animals (Fig. 4h, i). The synergistic effect was particularly evident in the case of the stunted-growth phenotype (Fig. 4h, i). The reduction of cilia length was, however, largely additive (Fig. 4j). The synergy between *rabaptin5*- and *elipsa*-knockdown confirms our finding that the protein products of these two genes bind to each other.

The small GTPase Rab8 localized to cilia in cultured cells; its constitutive activation resulted in an increase in cilia length, whereas interference with its function produced accumulation of intracellular vesicles at the base of the photoreceptor-connecting cilium[20,21]. Rab8 is thus a good candidate for the interaction partner of Rabaptin5 in ciliogenesis.

To test this idea, we performed double-knockdown of *rab8* and *rabaptin5*. RT-PCR of the target transcript from *rab8* morphants produced a barely detectable signal (Fig. 5i) and the double-morphant phenotype was partially eliminated by *rab8* mRNA at 2 days post-fertilization (dpf; Fig. 5h) and 4 dpf (data not shown), indicating that *rab8* knockdown is both efficient and specific. Again, we observed a marked synergistic enhancement of stunted growth and curly-body axis phenotypes in double morphant animals at 2 and 4 dpf (Fig. 5e, f). Knockdown of *rab8* also caused a slight decrease in ciliary length, which displayed synergy with *rabaptin5* knockdown (Fig. 5a–d, g). These observations suggest that Rabaptin5 may bind to Rab8 and act as its effector.

Rabaptin5 was previously shown to bind Rab4 and Rab5 through its N- and C-termini, respectively[11]. To test whether Rab8 binds to Rabaptin5, we first used the yeast two-hybrid system. Similarly to the studies of Rab4 and Rab5, these experiments revealed that full-length human Rabaptin5 bound to the constitutively active mutant Rab8Q67L, but not the wild-type or dominant negative Rab8T22N (Fig. 5j). An N-terminal Rabaptin5 fragment of 467 amino acids was sufficient to mediate these interactions (data not shown). Moreover, in a GST pulldown assay Rab8–GST bound to the N-terminal portion (amino acids 1–421) of the Rabaptin5–MBP fusion protein (Fig. 5k). Taken together, these findings support a model in which the Elipsa–Rabaptin5 complex provides a bridging mechanism between the IFT particle and membrane-associated Rab8 (Fig. 5n).

Our data suggest that Elipsa–Rabaptin5–Rab8 complex may mediate IFT-particle interactions with ciliary membrane proteins. To investigate this possibility, we analysed the localization of several ciliary transmembrane proteins. OSM-9, a TRPV channel, was previously shown to display abnormal distribution in IFT mutants[7]. We found that OSM-9 accumulated in distal dendritic ends of the OLQ ciliated neurons in *dyf-11* animals
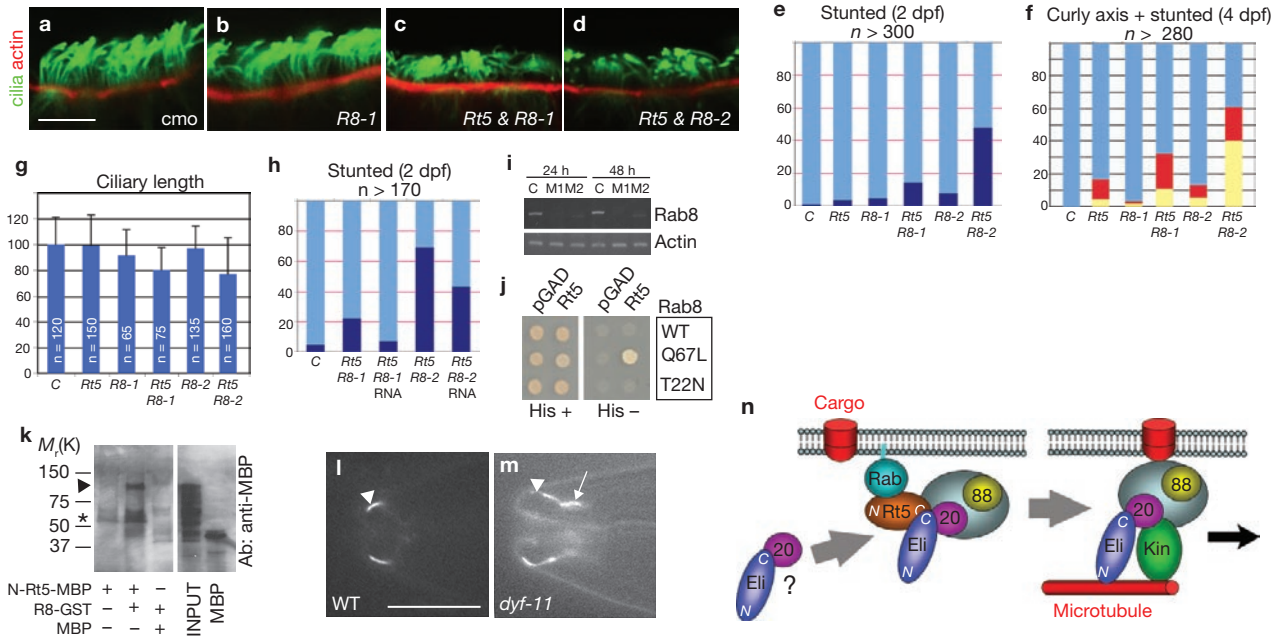
Figure 5 Rabaptin5 interacts with Rab8 genetically and biochemically. (**a**–**d**) Nasal cilia visualized with an anti-acetylated tubulin antibody (green) in embryos treated with the following MOs: cmo, control; *Rt5*, anti-*rabaptin5*; *R8-1* and *R8-2*, anti-*rab8* splice site MOs 1 and 2, respectively. Embryos were counterstained with phalloidin (red). (**e**–**g**) Quantification of phenotypes shown in **a**–**d**. The MOs injected are indicated below each graph. In panel **f**, bars are colour-coded as explained in Fig. 4. In **g**, the length of olfactory placode cilia was calculated in arbitrary units and expressed as a percentage of the WT value, which was set to 100% (data from four independent experiments). Data are mean ± s. d.; *n* = total number of cilia examined. (**h**) Rescue of *rab8* morphant phenotype. RNA is *rab8* mRNA. (**i**) RT-PCR quantification of knockdown efficiency for two anti-*rab8* splice site MOs (M1, M2). Sequencing of residual aberrant transcripts revealed that they contain premature translation termination codons. (**j**) Yeast two-hybrid tests of binding interactions between Rabaptin5 with Rab8. Three forms of the Rab8 protein were used: WT, a constitutively active mutant (Q67L), and a dominant negative mutant (T22N) (pGAD, empty vector control). (**k**) Western blot of Rab8–GST pulldown product, stained with an anti-MBP antibody. Input is 5% of the total MBP–Rabaptin5 input. Arrowhead indicates the full-length MBP–Rabaptin5 band. The lower band (asterisk) is a degradation product also seen in MBP–Rabaptin5 protein preparation (data not shown). (**l**, **m**) Localization of GFP-tagged OSM-9 TRPV channel in the cilia of *C. elegans* OLQ neurons in WT (**l**, arrowhead) and *dyf-11* mutants (**m**, arrowhead). The signal extends to the distal dendritic ends in *dyf-11* mutants (arrow). Anterior is to the left. (**n**) A model of Elipsa function. Elipsa is thought to have two roles in cilia: first, it mediates interaction between the Ift20 polypeptide and the membrane-bound Rab8 GTPase; second it may facilitate the IFT particle movement along the ciliary axoneme, possibly contributing to its interaction with ciliary microtubules. Elipsa may also act at stages preceding IFT. Scale bars are 10 μm (**a**–**d**) and 15 μm (**l**–**m**).

(Fig. 5l, m). The length of ciliary and/or dendritic processes occupied by OSM-9 in wild-type and *dyf-11* animals was 3.9 ± 0.4 μm (*n* = 33) and 9.0 ± 1.8 μm (*n* = 21), respectively. Interestingly, this phenotype is similar to that described for OSM-9 in *bbs-8* mutants[22]. Mislocalization of OSM-9 may have several causes, including an abnormal interaction of the OSM-9 protein with the IFT particle or, alternatively, a defect at an earlier stage of OSM-9 transport into cilia. A general defect of apicobasal polarity in *elipsa* (*dyf-11*) mutant cells is unlikely, however, given that the ciliary distributions of ODR-10, SRU-38, and Polycystin 2 are normal (Supplementary Information, Fig. S5), and the localizations of two major determinants of apicobasal polarity in zebrafish, aPKC and Crumbs were also unaffected (Supplementary Information, Fig. S6). Finally, we did not detect abnormalities in the Golgi apparatus of *C. elegans* ciliated neurons (Supplementary Information, Fig. S5g, h).

A possible reason for the early appearance of its mutant phenotype is that Elipsa may function before IFT-particle assembly, perhaps by interacting with Ift20 (Fig. 5n). Such a hypothesis is consistent with the findings that Ift20 is detected in the Golgi apparatus[23], and its knockdown in zebrafish also produces an earlier phenotype, compared with that of oval. The Ift20–Elipsa complex may be difficult to detect in *oval* mutants because it exists transiently, unless incorporated into the IFT particle. Furthermore, Rabaptin5 seemed to accumulate in punctate structures that may represent vesicles next to the base of the cilium (Fig. 3h, i). Thus in one model, Ift20 and Elipsa may first bind to each other, possibly form a complex with Rabaptin5 and only subsequently become incorporated into the IFT particle (Fig. 5n). Finally, it is worth noting that Elipsa was shown to bind to polymerized microtubules[24] and Ift20 to Kinesin[25]. It is thus possible that Elipsa also stabilizes the interaction of the IFT particle with axonemal microtubules (Fig. 5n).

Both Rab8, and Rabaptin5 are well conserved in vertebrates and their orthologues can also be identified in invertebrate phyla, suggesting that Rab8–Rabaptin5–Elipsa interactions may be universal (Supplementary Information, Fig. S1). These interactions may bring the IFT particle into the proximity of proteins embedded in the ciliary membrane or in the membrane of cytoplasmic transport vesicles. This work demonstrates for the first time a direct interaction between the IFT particle and a small GTPase pathway known to mediate the assembly of protein complexes at cell membranes[18]. Although suggested by previous studies[26], such interactions had not been reported to date. □

METHODS

Zebrafish strains. The breeding and maintenance of zebrafish strains and staging of embryonic development were performed as described previously[27]. The *elipsa*[m649] and *elipsa*[tp49d] alleles were originally recovered in the course of large-scale chemical mutagenesis screens[8,28].

Nematode strains and transgenics. The *dyf-11*(*mn392*) strain was obtained from the *Caenorhabditis* Genetics Center. A functional *gfp*-tagged *dyf-11* (*C02H7.1*) fusion gene was generated by fusing *gfp* coding sequences in frame to *dyf-11* genomic sequences, including approximately 3 kb of upstream regulatory sequences. *gfp*-tagged *sru-38*, *gfp*-tagged *odr-10*, and *osm-9::gfp3* have been described previously[29–31]. *osm-6p::mannosidase* (*mans*)–*YFP* was constructed by fusing approximately 2.4 kb of *osm-6* upstream sequences with *mans*–*YFP* sequences[32]. Concentrations of injected constructs were as follows: *gfp*-tagged *sru-38* and *gfp*-tagged *odr-10*, 30 ng μl⁻¹; *osm-9::gfp3*, 20 ng μl⁻¹ and *osm-6p::mans-YFP*, 5 ng μl⁻¹.

Imaging of *C. elegans* cilia. For quantification of IFT particle and motor movement, transgenic animals were anaesthetized with levamisole (10 mM) and mounted on agarose pads before imaging. Supplementary Information, Movie 1 was obtained with a Nikon Eclipse TE2000 microscope equipped with a ×100 (1.4 NA) objective and a forced air-cooled Photometrics Cascade 512B camera with a CCD87 CCD at 200 ms frame⁻¹. Kymographs and movies were generated using the Metamorph software package (Molecular Devices). Supplementary Information, Movie 2 was obtained with a Zeiss Axiovert 200M microscope equipped with a ×100 (1.3 NA) objective, a Yokogawa CSU22 spinning disk confocal head and a forced air-cooled Photometrics Cascade II 512 camera at 100 ms frame⁻¹. Kymographs and movies were generated using the Slidebook software package. Confocal images of *osm-6p::mans–YFP* were acquired using a Leica spectral confocal microscope equipped with ×100 (1.4 NA) objectives.

Cloning, MO-knockdown and phenotype rescue. A map cross was set up between heterozygous carriers of the *elipsa*[m649] allele (AB genetic background) and wild-type WIK strain homozygotes. To determine the segregation pattern of genomic polymorphisms, F2 embryos were genotyped as described previously[5]. The full-length cDNA of *elipsa* was amplified by RT-PCR using primers: CACAGAATAAACATCTTACATCCG and TGACTCTTGACTGTACCTGT AACC. Mutations were detected by direct sequencing of PCR products amplified from both genomic DNA and cDNA. The following MOs were used in knockdown experiments: *elipsa*–ATG, GGCTACCGATTCGTTCATGGCATCA; *rabaptin5*–SP, CTTGTGGAAGAAAACGCCTACCGTC; *ift20*–SP, CAACAACGTAC CTTCATTTTTTCAG; *rab8*–SP1, GAAGACATAAATACCTATCGTCGAG; *rab8*–SP2, GAGCATTGTCTTACCATTGCACCTC. To rescue mutant and morphant phenotypes, the full-length sequences of *elipsa*, *ift20*, *rabaptin5*, and *rab8* were cloned into the pXT7 vector[27] and transcribed using mMessage mMachine kit (Ambion), according to manufacturer's instructions. Approximately 40 pg of RNA was injected into embryos at the one-cell stage.

Immunohistochemistry. Fixation, infiltration, sectioning of embryos and other steps of antibody staining procedure were described previously[5]. The following primary antibodies and dilutions were used: mouse anti-acetylated-α-tubulin (1:500, Sigma), mouse anti-γ-tubulin (1:500, Sigma), rabbit anti-GFP (1:300, Clontech) and rabbit anti-Rabaptin5 (1:100, SantaCruz). The staining of hair cells and pronephric cilia was performed as described previously[33].

Yeast two-hybrid experiments. The ORF of the *elipsa* cDNA (full length or amino acids 330–629) was inserted into the pGBKT7 bait vector and transformed into the AH109 yeast strain. We screened 2.5 × 10⁶ transformants from mouse 17-day embryo cDNA library (Clontech) according to Clontech instructions for Matchmaker System 3. Positive colonies were identified on the basis of their ability to express the nutritional markers HIS3 and ADE2. To test whether Elipsa binds to Rabaptin5 and Ift20, full-length Elipsa or its C-terminal fragments were cloned into pGBKT7 bait vector (Clontech) whereas mouse Ift20 and mouse Rabaptin5 (amino acids 489–862) were cloned into pACT2 prey vector (Clontech). To test binding interactions between Rab8 and Rabaptin5, we used wild-type and mutant *rab8* sequences cloned into pBD–GAL4–Cam (Stratagene) bait vector (construct provided by J. Goldenring, Vanderbilt University School of Medicine, Nashville, TN) whereas full-length human Rabaptin5 or its N-terminal fragment of 467 amino acids were expressed from pGAD10 (Clontech) prey vector (construct provided by J. Bonifacino, National Institutes of Health, Bethesda, MD).

GST Pull-Down Experiments. We prepared the following fusion constructs: Elipsa-C–GST (amino acids 316–629) and Rab8–GST (full length) in pGEX-4T-1 vector; Ift20–MBP, mouse Rabaptin5–C-MBP (amino acids 546–862), human

Rabaptin5–N-MBP (amino acids 1– 421) in pMAL–c2X vector and Rabaptin5–HisTag (full-length zebrafish sequence) in pET-28a vector. To evaluate expression levels, fusion proteins in bacterial extracts were detected using Coomassie Blue staining on polyacrylamide gels. We purified His-tagged and MBP-tagged fusion proteins using HisPur cobalt resin (Pierce) and amylose resin (NEB), respectively. Purified MBP, Ift20–MBP, Rabaptin5–C-MBP or His–Rabaptin5 were incubated with GST or Elipsa–C-GST coupled to glutathione–Sepharose 4B beads (Amersham Biosciences) for 1 h at 4°C in binding buffer (50 mM Tris pH 7.5, 100 mM NaCl, 1 mM EDTA, 2 mM DTT, 0.5% Triton-X100). After two washes with the binding buffer, protein complexes were subjected to electrophoresis and detected by immunoblotting. Purified MBP or Rabaptin5–N-MBP were incubated with GST or Rab8–GST coupled to glutathione–Sepharose 4B beads for 30 min at room temperature in binding buffer (20 mM HEPES pH 7.0, 2 mM DTT, 100 mM NaCl, 0.5% TritonX-100) containing 100 μM GTPγS. After three washes with the binding buffer, bound proteins were separated by electrophoresis and detected by immunoblotting.

TAP. ProteinA/CBP TAP tag[34] was fused to the C-terminus of GFP–Elipsa (pXT7–GFP–Elipsa–CTAP). Using this construct as a template, mRNA was synthesized *in vitro* with mMessage mMachine kit (Ambion) and injected into approximately 7000 embryos at the one-cell stage. Embryos were collected at 30 hpf and homogenized in lysis buffer. Purification of Elipsa protein complexes from embryo extracts was performed using protocols published previously[34]. The identity of purification products was determined using LC-MS/MS mass spectrometry (Taplin Facility, Harvard Medical School). In addition to IFT particle components, this analysis identified a number of proteins that are known to purify non-specifically in this procedure, such as heat-shock and cytoskeletal proteins (data not shown).

Note: Supplementary Information is available on the Nature Cell Biology website.

1. Kozminski, K. G., Beech, P. L. & Rosenbaum, J. L. The *Chlamydomonas* kinesin-like protein FLA10 is involved in motility associated with the flagellar membrane. *J. Cell Biol.* **131**, 1517–1527 (1995).
2. Rosenbaum, J. L. & Witman, G. B. Intraflagellar transport. *Nature Rev. Mol. Cell Biol.* **3**, 813–825 (2002).
3. Singla, V. & Reiter, J. F. The primary cilium as the cell's antenna: signaling at a sensory organelle. *Science* **313**, 629–633 (2006).
4. Eggenschwiler, J. T. & Anderson, K. V. Cilia and developmental signaling. *Annu. Rev. Cell Dev. Biol.* **23**, 345-373 (2007).
5. Tsujikawa, M. & Malicki, J. Intraflagellar transport genes are essential for differentiation and survival of vertebrate sensory neurons. *Neuron* **42**, 703–716 (2004).
6. Orozco, J. T. *et al.* Movement of motor and cargo along cilia. *Nature* **398**, 674 (1999).
7. Qin, H. *et al.* Intraflagellar transport is required for the vectorial movement of TRPV channels in the ciliary membrane. *Curr. Biol.* **15**, 1695–1699 (2005).
8. Malicki, J. *et al.* Mutations affecting development of the zebrafish retina. *Development* **123**, 263–273 (1996).
9. Doerre, G. & Malicki, J. Genetic analysis of photoreceptor cell development in the zebrafish retina. *Mechanisms of Development* **110**, 125–138. (2002).
10. Avidor-Reiss, T. *et al.* Decoding cilia function: defining specialized genes required for compartmentalized cilia biogenesis. *Cell* **117**, 527–539 (2004).
11. Vitale, G. *et al.* Distinct Rab-binding domains mediate the interaction of Rabaptin-5 with GTP-bound Rab4 and Rab5. *EMBO J.* **17**, 1941–1951 (1998).
12. Stenmark, H., Vitale, G., Ullrich, O. & Zerial, M. Rabaptin-5 is a direct effector of the small GTPase Rab5 in endocytic membrane fusion. *Cell* **83**, 423–432 (1995).

13. Starich, T. A. *et al.* Mutations affecting the chemosensory neurons of *Caenorhabditis elegans. Genetics* **139,** 171–188 (1995).
14. Perkins, L. A., Hedgecock, E. M., Thomson, J. N. & Culotti, J. G. Mutant sensory cilia in the nematode *Caenorhabditis elegans. Dev. Biol.* **117,** 456–487 (1986).
15. Ou, G. *et al.* Sensory ciliogenesis in Caenorhabditis elegans: assignment of IFT components into distinct modules based on transport and phenotypic profiles. *Mol. Biol. Cell* **18,** 1554–1569 (2007).
16. Kunitomo, H. & Iino, Y. *Caenorhabditis elegans* DYF-11, an orthologue of mammalian Traf3ip1/MIP-T3, is required for sensory cilia formation. *Genes Cells* **13,** 13–25 (2008).
17. Snow, J. J. *et al.* Two anterograde intraflagellar transport motors cooperate to build sensory cilia on C. elegans neurons. *Nature Cell Biol.* **6,** 1109–1113 (2004).
18. Grosshans, B. L., Ortiz, D. & Novick, P. Rabs and their effectors: achieving specificity in membrane traffic. *Proc. Natl Acad. Sci. USA* **103,** 11821–11827 (2006).
19. McBride, H. M. *et al.* Oligomeric complexes link Rab5 effectors with NSF and drive membrane fusion via interactions between EEA1 and syntaxin 13. *Cell* **98,** 377–386 (1999).
20. Moritz, O. L. *et al.* Mutant *rab8* impairs docking and fusion of rhodopsin-bearing post-Golgi membranes and causes cell death of transgenic *Xenopus* rods. *Mol. Biol. Cell* **12,** 2341–2351 (2001).
21. Nachury, M. V. *et al.* A core complex of BBS proteins cooperates with the GTPase Rab8 to promote ciliary membrane biogenesis. *Cell* **129,** 1201–1213 (2007).
22. Tan, P. L. *et al.* Loss of Bardet Biedl syndrome proteins causes defects in peripheral sensory innervation and function. *Proc. Natl Acad. Sci. USA* **104,** 17524–17529 (2007).
23. Follit, J. A., Tuft, R. A., Fogarty, K. E. & Pazour, G. J. The intraflagellar transport protein IFT20 is associated with the Golgi complex and is required for cilia assembly. *Mol. Biol. Cell* **17,** 3781–3792 (2006).
24. Ling, L. & Goeddel, D. V. MIP-T3, a novel protein linking tumor necrosis factor receptor-associated factor 3 to the microtubule network. *J. Biol. Chem.* **275,** 23852–23860 (2000).
25. Baker, S. A., Freeman, K., Luby-Phelps, K., Pazour, G. J. & Besharse, J. C. IFT20 links kinesin II with a mammalian intraflagellar transport complex that is conserved in motile flagella and sensory cilia. *J. Biol. Chem.* **278,** 34211–34218 (2003).
26. Jekely, G. & Arendt, D. Evolution of intraflagellar transport from coated vesicles and autogenous origin of the eukaryotic cilium. *Bioessays* **28,** 191–198 (2006).
27. Malicki, J., Jo, H., Wei, X., Hsiung, M. & Pujic, Z. Analysis of gene function in the zebrafish retina. *Methods* **28,** 427–438. (2002).
28. Brand, M. *et al.* Mutations affecting development of the midline and general body shape during zebrafish embryogenesis. *Development* **123,** 129–142 (1996).
29. Colosimo, M. E. *et al.* Identification of thermosensory and olfactory neuron-specific genes via expression profiling of single neuron types. *Curr. Biol* .**14,** 2245–2251 (2004).
30. Sengupta, P., Chou, J. H. & Bargmann, C. I. *odr-10* encodes a seven transmembrane domain olfactory receptor required for responses to the odorant diacetyl. *Cell* **84,** 899–909 (1996).
31. Colbert, H. A., Smith, T. L. & Bargmann, C. I. OSM-9, a novel protein with structural similarity to channels, is required for olfaction, mechanosensation, and olfactory adaptation in *Caenorhabditis elegans. J Neurosci* **17,** 8259–8269 (1997).
32. Rolls, M. M., Hall, D. H., Victor, M., Stelzer, E. H. & Rapoport, T. A. Targeting of rough endoplasmic reticulum membrane proteins and ribosomes in invertebrate neurons. *Mol. Biol. Cell* **13,** 1778–1791 (2002).
33. Omori, Y. & Malicki, J. *oko, meduzy* and related *crumbs* genes are determinants of apical cell features in the vertebrate embryo. *Curr. Biol.* **16,** 945–957 (2006).
34. Veraksa, A., Bauer, A. & Artavanis-tsakonas, S. Analyzing protein complexes in *Drosophila* with tandem affinity purification–mass spectrometry. *Dev. Dynamics* **232,** 827–834 (2005).
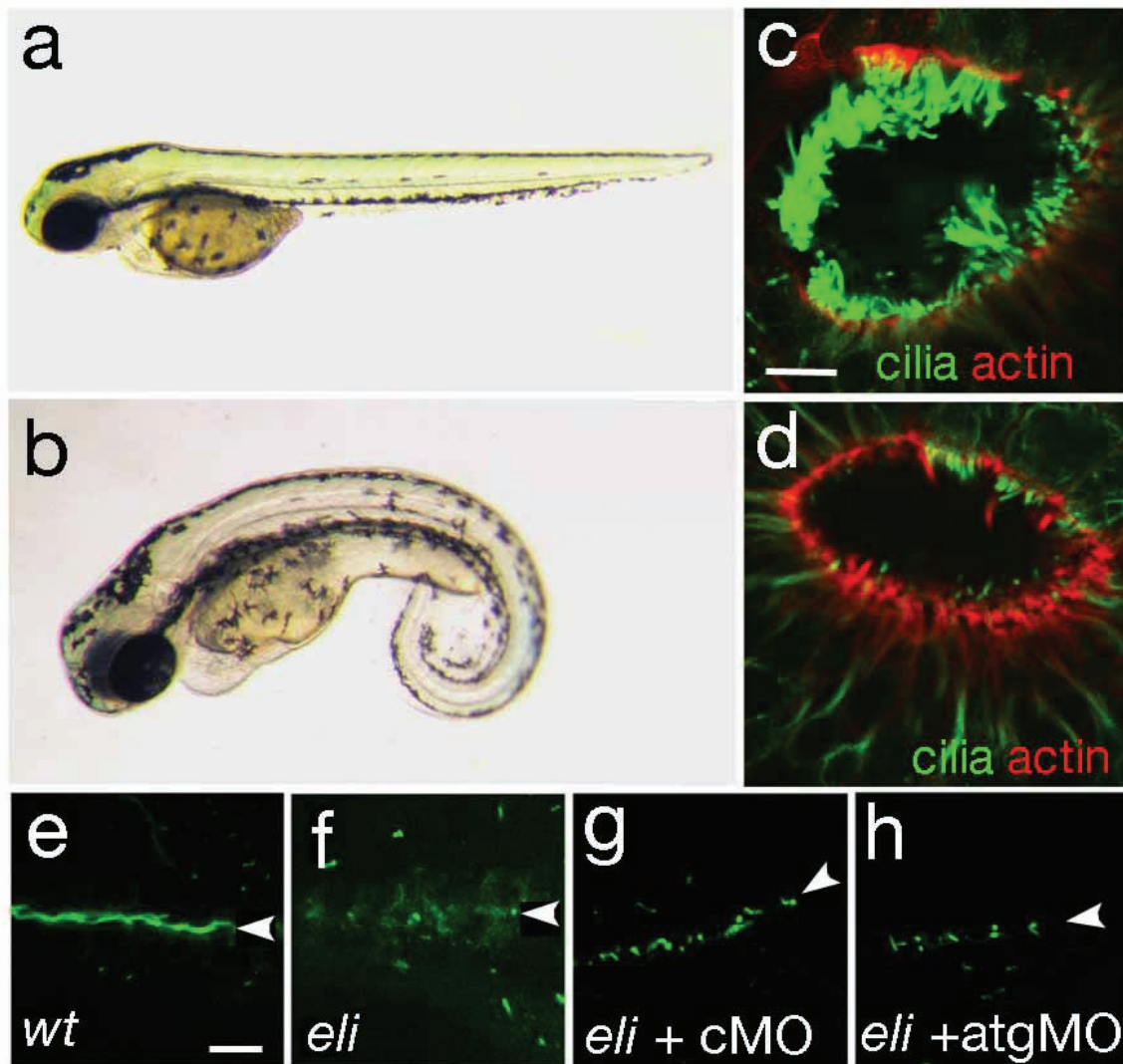
Figure S1 Elipsa, Rabaptin 5, and Rab8 homologs in other phyla. **a,** Evolutionary relationships between *elipsa* homologs in different phyla. **b,** Sequence alignment of the *elipsa* N-terminus in zebrafish, human, fly, and nematode genes. The *elipsa*[m649] mutant allele carries an Isoleucine to Asparagine substitution at the position 17 (color coded in red). This position is very well conserved in evolution. The phenotype of this mutant allele is characterized by a somewhat less severe body curvature, compared to *eli*[tp49d], which introduces a stop codon. **c,** ClustalW alignment of human and zebrafish *elipsa* sequences. The best conserved protein regions are color-coded in red and blue. **d,** Evolutionary tree of Rabaptin5 protein sequence from several phyla. Putative Rabaptin5 orthologs from invertebrates are only distantly related to vertebrate sequences. **e,** Evolutionary tree of Rab8 protein sequence from several phyla. In **a**, **d**, and **e**, GenBank accession code for each sequence is provided. Ce, Caenorhabditis elegans; Cr, Chlamydomonas reinhardi; Dm, Drosophila melanogaster; Hs, homo sapiens; Mm, Mus musculus.

Figure S2 Phenocopy of *elipsa* defect. **a,** A 3 dpf zebrafish larva treated with a control morpholino. No obvious phenotypic changes are present. **b,** The same treatment with anti-*elipsa* morpholino oligonucleotides induces a curled body axis in approximately 90% of larvae (Table S1). This phenotype closely resembles *elipsa* mutants (Fig. 1b). **c,** Olfactory pit cilia visualized by staining with anti-acetylated tubulin antibodies (green). The injection of a control morpholino does not result in any obvious changes of cilia appearance. **d,** The injection of anti-*elipsa* MO on the other hand into wild-type embryos produces a reduction of cilia number in nasal pit epithelia. **e-h,** To test the possibility that maternal contribution obscures the early aspects of *elipsa* mutant phenotype, we injected anti-ATG (atgMO) *elipsa* morpholino oligonucleotides into animals originating from crosses between *elipsa* heterozygotes. A non-specific morpholino (cMO) was used as a control. Kidney cilia visualized with anti-acetylated tubulin antibody (green) in wild-type (**e**), *elipsa*^{tp49d} mutant (**f**), *elipsa*^{tp49d} mutant treated with a control morpholino (**g**), and a presumptive *elipsa*^{tp49d} mutant treated with anti-ATG morpholino (**h**). No obvious difference was observed in cilia length or external morphology between anti-ATG and control morpholino-treated individuals. Arrowheads indicate the approximate location of the pronephric duct. In **a**, **b** anterior is left and dorsal is up. **c**, and **d** are counterstained with phalloidin (red signal). Scale bars are 10 μm.
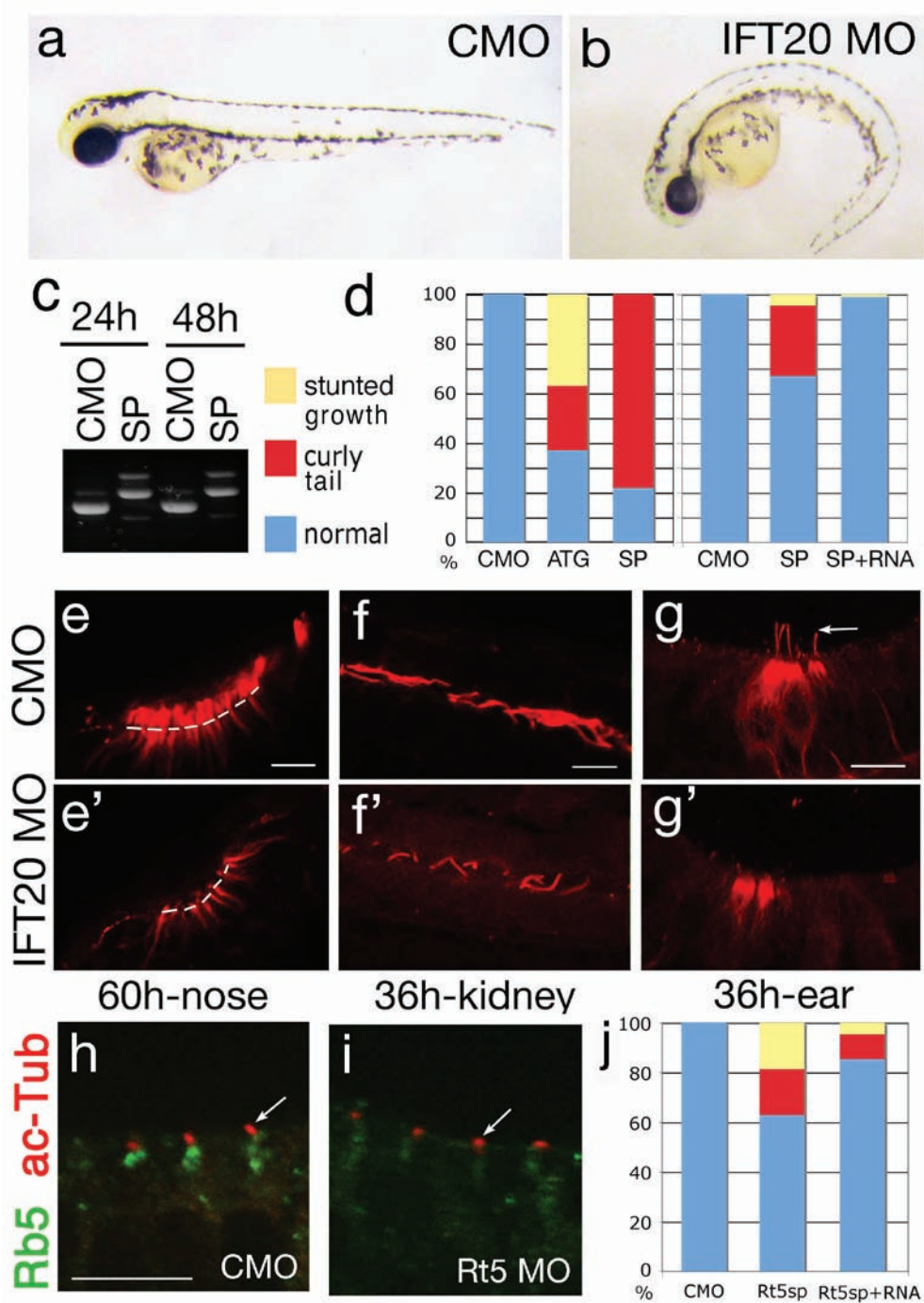
Figure S3 *ift20* and *rabaptin5* knockdowns. **a** and **b,** The phenotype of *ift20* morphant (**b**), compared to its sibling treated with a control morpholino (**a**). **c,** The efficiency of anti-*ift20* splice site morpholino as measured by RT-PCR. The wild-type transcript is not detectable in morphants at 24 and 48 hpf, and instead a longer amplification product is present. The sequencing of the longer product revealed an insertion of 69 bp. As this insertion does not result in a frameshift, the resulting protein product may be partially functional. **d,** The frequency of phenotypes in morpholino-treated embryos (left graph) and the rescue of morphant phenotype (right graph). For each experimental group, n≥65. Stunted animals display severely delayed growth at 3 dpf, as shown in Fig. 4g. **e - g',** Staining with an anti-acetylated-α-tubulin antibody of cilia in the olfactory pit (**e, e'**), the pronephric duct (**f, f'**), and the otic vesicle (**g, g'**) of embryos treated with anti-*ift20* morpholino (bottom row), compared to control morpholino-treated siblings (upper row). Arrow in (**g**) indicates hair cell kinocilia. White dashes in (**e**) indicate the base of cilia. **h - j,** efficiency and specificity of *rabaptin5* morpholino knockdown. Staining with anti-Rabaptin5 (green) and anti-acetylated α-tubulin (red) antibodies of control (**h**) and anti-*rabaptin5* (**i**) morpholino-treated embryos. Arrows indicate the localization of cilia (red signal). **j,** Rescue of *rabaptin5* morpholino knockdown phenotype by *rabaptin5* mRNA co-injection (n≥65). Phenotypes scored are as shown in Fig. 4. Scale bars are 10 μm. CMO, control morpholino; ATG, initiation codon-targeted morpholino; SP, splice site-targeted morpholino; RNA, *ift20* messenger RNA.
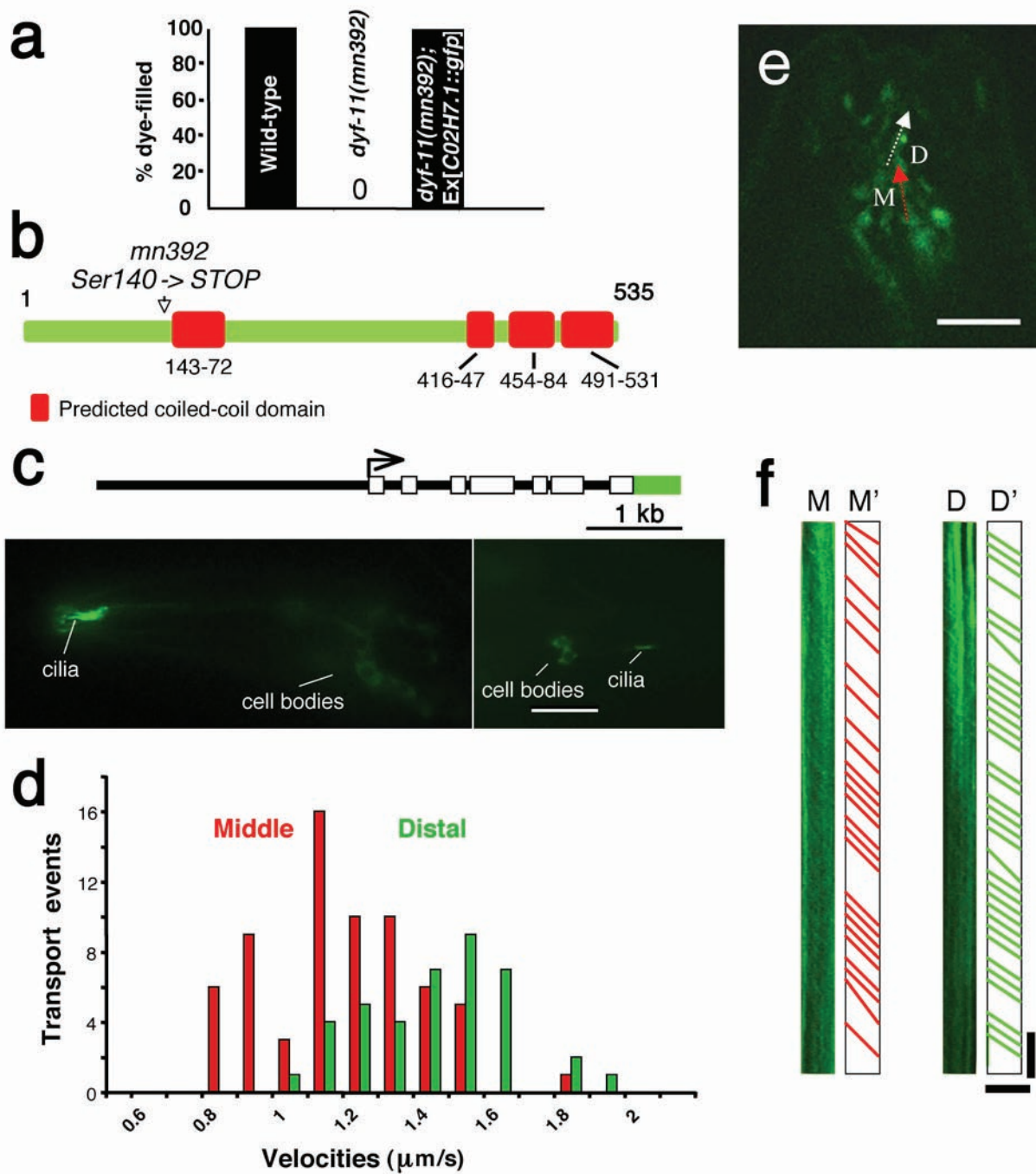
Figure S4 *elipsa* homolog in *C. elegans*. **a,** The *C. elegans elipsa* homolog *C02H7.1* rescues the dye-filling defects of *dyf-11(mn392)* mutants. Animals were filled with DiI. GFP-tagged C02H7.1 was injected at a concentration of 2 ng/μl. For each genotype, n >50. **b,** The genomic structure of C02H7.1. The locations of the predicted coiled-coil domains and the molecular nature of the *mn392* mutation are indicted. Coiled-coil domain predictions were made using a primary structure analysis program (http://npsa-pbil.ibcp.fr/cgi-bin/npsa_automat.pl?page=npsa_lupas.html). Not drawn to scale. **c,** The localization of functional GFP-tagged full-length C02H7.1 (DYF-11) in the cilia of sensory neurons in the head (amphid sensory neurons; left panel), and tail (phasmid sensory neurons; right panel). Expression is also observed in cell bodies likely due to overexpression of the fusion protein. Scale bar is 15 μm. Anterior is to the left. **d - f,** Anterograde transport of GFP-tagged DYF-11 in the cilia of sensory neurons in the head of *bbs-8* mutants. Shown are histograms of DYF-11::GFP velocities (**d**), a still image (**e**) and kymographs (**f**) from a representative movie of DYF-11 transport. Arrows on the still image indicate locations used to generate the kymographs along the middle (M) and distal (D) segments. Lines in M' and D' refer to kymographs shown in M and D used to calculate velocities. The average velocities are 1.20 ± 0.21 μm sec^{-1} in the middle segments (67 particles/4 examined cilia), and 1.44 ± 0.20 μm sec^{-1} in the distal segments (39 particles/3 examined cilia). Scale bar in (**e**) is 5 μm. Scale bars in kymographs: horizontal bar, 5 μm; vertical bar, 5s. The *bbs-8(nx77)* allele was used.
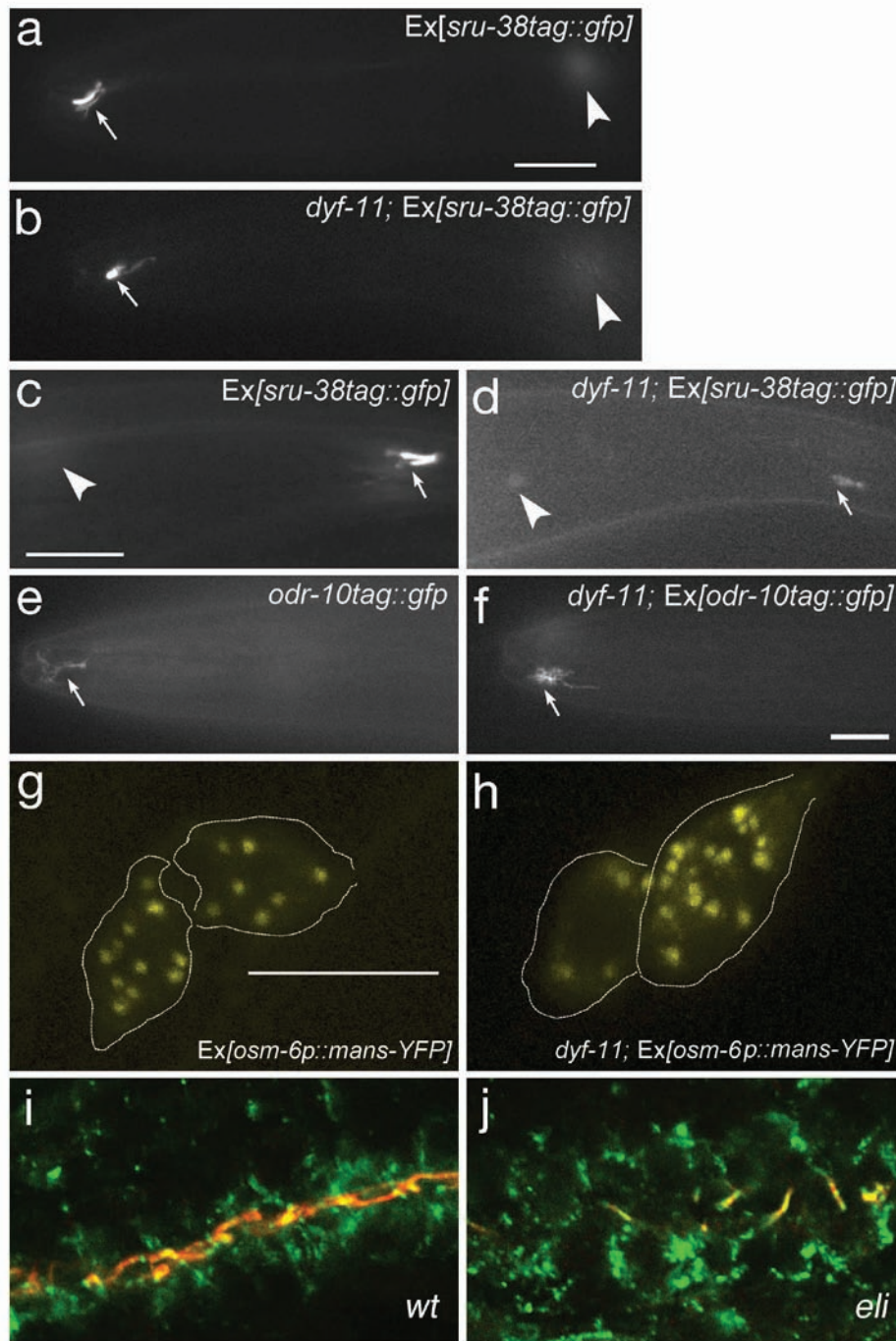
Figure S5 Localization of ciliary transmembrane proteins in C. elegans (**a**-**h**) and zebrafish mutants (**i**-**j**). **a** and **b**, Localization of GFP-tagged SRU-38 chemoreceptor protein in the cilia of the AWB and ASH chemosensory neurons in wild-type (**a**) and *dyf-11* mutants (**b**). SRU-38 retains ciliary localization in *dyf-11* mutants with shortened cilia. **c** and **d**, Localization of GFP-tagged SRU-38 in the cilia of PHA/B phasmid neurons in the tail of wild-type (**c**) and *dyf-11* mutants (**d**). **e** and **f**, Localization of GFP-tagged ODR-10 chemoreceptor protein in the cilia of the AWA olfactory neurons in the wild-type (**e**) and *dyf-11* mutants (**f**). In **a** - **f** arrows indicate cilia, arrowheads indicate cell bodies. Scale bar is 15 μm. **g** and **h**, Golgi bodies in the phasmid neurons of wild-type (**g**) and *dyf-11* (**h**) animals visualized using a mannosidase-YFP marker [32]. The boundaries of phasmid neuron cell bodies are outlined. Maximal projections from stacks of confocal images are shown. Scale bar is 7.5 μm. *dyf-11(mn392)* animals were examined. **i** and **j**, Double staining of the zebrafish pronephric duct with antibodies to Polycystin 2 (green), and acetylated α-tubulin (red) in wild-type (**i**) and *elipsa* (**j**) animals. In **a** - **f**, anterior is to the left.
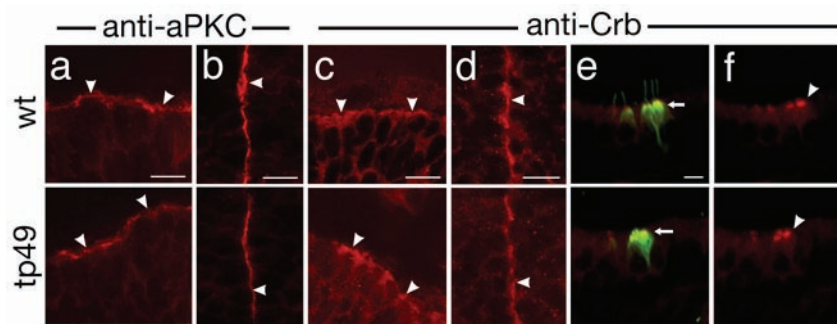
Figure S6 The distribution of apical determinants in *elipsa* mutants. **a - d**, Confocal images of cryosections through the zebrafish retina (**a**, **c**) and brain (**b**, **d**) stained with antibodies to aPKC (**a, b**) and Crumbs (**c, d**). Arrowheads indicate the apical surface. **e** and **f**, Confocal images of the zebrafish otic vesicle in whole embryos stained with antibodies to the Crumbs protein (red), and acetylated α-tubulin (green, panel **e** only). The Crumbs polypeptide accumulates at the apical termini of auditory hair cells (arrowheads), here visualized via elevated acetylated α-tubulin signal (arrows). Wild-type individuals are shown in the upper row of images, *elipsa*^{tp49d} mutant embryos in the lower row. Scale bars are 10 μm.

Supplementary Movie legends

Movie S1 Transport of GFP-tagged C02H7.1::GFP in the sensory cilia of wild-type *C. elegans.* The display rate is 5 frames sec^{-1} with the total elapsed time of 40 sec.

Movie S2 Transport of GFP-tagged C02H7.1::GFP in the sensory cilia of *bbs-8(nx77)* mutant *C. elegans*. The display rate is 10 frames sec^{-1} with the total elapsed time of 65 sec.

Supplementary Data

Table S1. Phenocopy of *elipsa* defect.

Morpholino Injected	Body Axis (3dpf)		Nasal Cilia (3dpf)	
	Curved	Normal	Defective	Normal
Control	0%(0/58)	100%(58/58)	0%(0/20)	100%(20/20)
elipsa-ATG-MO	90.2%(37/41)	9.8%(4/41)	90.3%(28/31)	9.7%(3/31)

Embryos were injected with morpholino oligonucleotides as indicated. The injection of anti-*elipsa* morpholino results in a curly tail phenotype and a loss of olfactory pit cilia in approximately 90% of larvae at 3 dpf . By contrast, treatment with a control morpholino does not appreciably affect wild-type phenotype.

Table S2. Phenotypic rescue of *elipsa* mutants via mRNA injection.

mRNA injected	Body Axis (3dpf)	
	Curved	Normal
GFP	22%(17/76)	78%(59/76)
GFP-elipsa	0%(0/87)	100%(87/87)

Embryos from crosses between *elipsa* heterozygotes were treated with in vitro synthesized mRNA as indicated. As expected, approximately one fourth of larvae treated with control GFP mRNA display curly tail at 3dpf. In contrast, all larvae treated with *elipsa* mRNA feature a normal shape of body axis.

Table S3. Peptide sequences identified through mass spectrometric analysis of TAP products.

ID	Identified proteins	position	peptide sequence
gi|50539690	**Ift172**	886-894	AIEAAIAAR
		31-38	FAVCTIDR
		1563-1571	HTELIPADK
		1480-1488	MFQELVNLR
		1679-1691	SLPCVITGYPVLR
		225-236	EGNVIQTFDYSR
		1664-1678	GTYEASLVAASTGIR
gi|50539694	**Ift81**	543-550	STLEQEVR
		231-239	NQLFQAEQR
		298-310	VASEPAMGQAELR
		603-615	YIANTAEQESLGK
		438-452	HTAGQQQLQSLEAQR
gi|56693322	**Ift80**	487-494	DLYLTSVR
		439-449	VVFLFEAQTGK
gi|49227536	**Ift57**	361-371	LKQEIEQMDVR
		306-320	VKELYQQASGGVTER
gi|108935969	**Qilin**	191-200	DVTESIQMTK
		169-183	TAAIARPLEITETER
gi|56118556	**Ift20**	21-29	VLEPDVSQK
		50-63	IVGGLIELVDELAK
		30-43	TTELKEECEEFVDK
		87-100	EAQQQQLQALIAEK
		117-132	VEAEQSEFIDQFILQK